Pore Wall Thinning of Mesoporous 4H-SiC by Sacrificial Oxidation

Marzaini Rashid[*,1], Muhammad Idzdihar Idris[2,3], Benjamin Horrocks[4], Noel Healy[3], Jonathan Paul Goss[3], and Alton Barrett Horsfall[5].

[1] School of Physics, Universiti Sains Malaysia, 11800 USM, Penang, Malaysia.
[2] Faculty of Electronic and Computer Engineering, UTeM, Hang Tuah Jaya, 76100 Durian Tunggal, Melaka, Malaysia.
[3] School of Engineering, Newcastle University, Newcastle NE1 7RU, United Kingdom.
[4] School of Natural Environmental Sciences, Newcastle University, Newcastle NE1 7RU, United Kingdom.
[5] Department of Engineering, University of Durham, DH1 3LE, United Kingdom.

Abstract

Pore wall thinning of mesoporous 4H-SiC by sacrificial oxidation has been performed. The dimensions within the as-etched porous SiC are reduced during dry oxidation at 1100°C by consuming SiC and removing the grown SiO_2 in the subsequent HF dip step. The process reduces the average pore wall thickness from 27 nm to approximately 16 nm and reduces the thickness standard deviation from ±5 nm to ±1.4 nm for the investigated 9 hour oxidation interval. The new pore wall thinning method will enable controlled nanoscale size reduction capability for mesoporous 4H-SiC derived nanostructures.

1 Introduction There is significant interest in nano- materials as new avenues to enable tailoring of fundamental material properties at the length scales these properties are determined. [1]

The fundamental properties of nanostructures that distinguish them from their bulk counterparts include in- creased energy in the optical properties as a result of quantum confinement effects [2]. The quantum size effects occur at length scales close to the exciton Bohr radius, where the energy gap increases with decreasing particle size [3].

Quantum dots (QDs) and ultrasmall nanocrystals can be derived from porous structures via a two step process; anodic electrochemical etching to produce porous structures followed by ultrasonication of the porous material. This is the favoured method in producing SiC nanocrystals with ultrasmall sizes owing to advantages in the lower cost, simplicity in experimental setup, ambient pressure and room temperature processing that result in high crystallinity of the obtained nanocrystals [4–7]. Pioneering work by Shor *et al.* [8] first reported on porous SiC forma- tion by anodizing *n*-type 6H-SiC in HF under UV illumination in a Teflon electrochemical cell. Mesoporous structures with pore sizes of 10-30 nm with interpore spacings of 5-150 nm were reported. Ke *et al.* [9] performed anodic electrochemical etching of *n*-type 6H-SiC and showed that nano-columnar pores of ~20 nm diameter can be achieved by using a voltage bias of 20 V.

In previous work, SiC QDs were fabricated by anodic electrochemical etching and ultrasonication of poly- crystalline 3C-SiC in HF/ethanol (HF/C_2H_5OH, 2:1 ratio) [4]. The process included etching of 1 hour at a cur- rent density of 60 mA/cm^2 followed by ultrasonication of the obtained porous SiC. The etching and ultrasonication processes were repeated another two times in order to completely separate small nanocrystallites from the porous structure. The resulting 3C-SiC nanocrystals were in the size range of 1-6 nm. The PL emission peak maximum, ranged from 440 nm to 560 nm for excitation wavelengths of 320 nm to 490 nm which was the first experimental evidence of quantum confinement in 3C-SiC QDs.

However, producing nanoscale QDs with high yield is non-trivial for porous SiC derived nanoparticles. Additional laborious steps are required in order to break porous SiC into the desired average size and yield. Larger crystallites are disposed of after filtration or centrifugation. A potential resolution via atmospheric pressure plasma processing using tetramethylsilane (TMS) as precursor has been explored for bottom-up synthesis of SiC QDs and has shown high yield with a mean diameter of 1.5 nm within a narrow size distribution [10]. The process however requires the use of specialised equipment for silane based plasma processing.

A potential alternative route to improve the yield and further downsize electrochemically etched SiC porous structures is by adding a sacrificial oxidation step. In sacrificial oxidation, the dimensions within the as-etched porous SiC are further reduced during oxidation by consuming SiC and the subsequent HF dip step removes the grown SiO_2. In recent work for porous Si, nanoparticles smaller than 6 nm were obtained from porous Si after pore-wall thinning using an oxidation step [11] followed by sonication which was otherwise difficult to achieve with sonication alone. It was hypothesized that

the surface energy barrier to form particles increases with reducing particle size and eventually sonication would not be sufficiently powerful to reduce the dimensions further. In another work, the fracture energy required to break a nanometer-sized particle is larger than a micrometer-sized one [12] during bubble collapse in ultrasonication. This follows the idea that the pore wall thickness in the porous structure determines the minimum particle size that can be achieved by sonication or mechanically driven top-down approaches. Pored SiC has found applications as catalysts supports, biosensors, supercapacitors, nanoporous membranes, nanofilters, as well as a starting material to produce SiC nanoparticles [13]. Control of pore morphology and pore wall thickness in the conventional electrochemical etching may be less predictable due to the high etching rate and dependence on etching conditions [14, 15]. As such, the sacrificial oxidation step with low etching rate may compensate this effect and will benefit these applications in providing better control of porous SiC dimensions. In this work the pore wall thinning of electrochemically etched porous SiC by sacrificial oxidation is performed as a new means to reduce dimensions of porous SiC.

2 Methodology Mesoporous 4H-SiC was prepared by anodic electrochemical etching of a *n*-type, 8° cut off the c-axis ([0001]), 4H-SiC wafer piece in 48% HF/ethanol (1:1 by volume) for 1 hour at an applied bias of 20 V using a Keithley 2611A source meter as described in previous work [16]. The etching time of 1 hour at 20 V was sufficiently long to delaminate the porous layer. The resulting as-etched delaminated mesoporous 4H-SiC film (D-Por- SiC) was removed from the wafer. Pore wall thinning and oxide removal by sacrificial oxidation of the D-Por- SiC was performed by a two step process: dry oxidation and SiO_2 removal in 48% HF/ethanol. After anodic electrochemical etching and drying of the D-Por-SiC in air, the material was thermally oxidised in dry oxygen with a flow rate of 100 sccm at 1100°C. Thermal oxidation durations of 1, 3, 6 and 9 hours were employed. After thermal oxidation, the oxidised D-Por-SiC were dipped in 48% HF/ethanol solution (1:1 by volume) for 5 minutes to remove the thermally grown SiO_2 followed by a rinse in ethanol and deionised water. The pore wall thinned D- Por-SiC is referred to as PWT-Por-SiC. D-Por-SiC layers were broken up by sonication and scanned using a high resolution transmission electron microscope (HRTEM) on a JEOL-2100F FEG TEM operated at 200 kV. PWT-Por- SiC samples were cleaved using tweezers and scanned along the broken edge in field emission scanning electron microscopy (FESEM) using a Phillips XL30 ESEM-FEG, to obtain cross-sectional images. The FESEM scans were performed at 10 kV with magnification of 50,000X.

3 Results and discussion Figure 1 shows the sur- face morphology of D-Por-SiC mesopores with average diameter of 33.3±7.8 nm and interconnected thin walls. The rough surface morphology of D-Por-SiC incorporated small feature sizes illustrating that numerous nanometer scale hexagonal shaped pores were evident throughout.

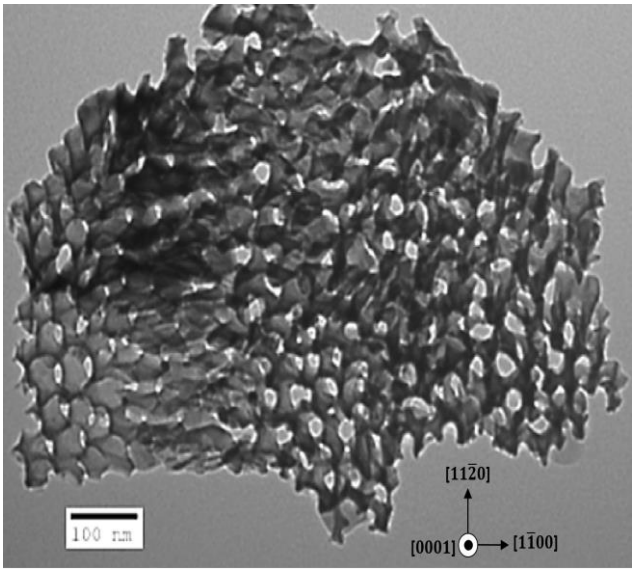

Figure 1 HRTEM image showing D-Por-SiC particle having a mesoporous structure. The crystal direction on the surface is (0001), in the plane of the image. It is nearly perpendicular to the c-axis [0001] direction (into the image) into which the pore channel propagates. Scale bar: 100 nm.

The pore diameter is a metric that can be used to classify the porous material. According to the International Union of Pure and Applied Chemistry (IUPAC) classification of pore size [17], pores with

diameters less than 2 nm are of the micro type, 2-50 nm are of the meso type and more than 50 nm are of the macro type. Pores with aver- age diameter of approximately 33.3±7.8 nm classifies the pores as mesopores. The pore diameter is consistent with previous work [9] that reported on a pore diameter of about 20 nm for 6H-SiC etched at 20 V.

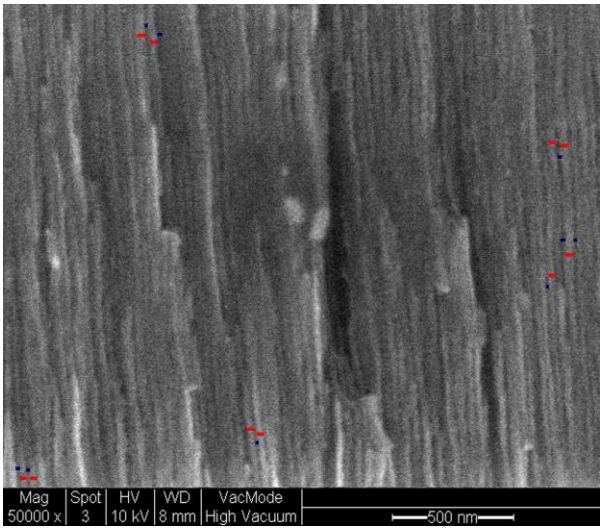

a) As-etched D-Por-SiC.

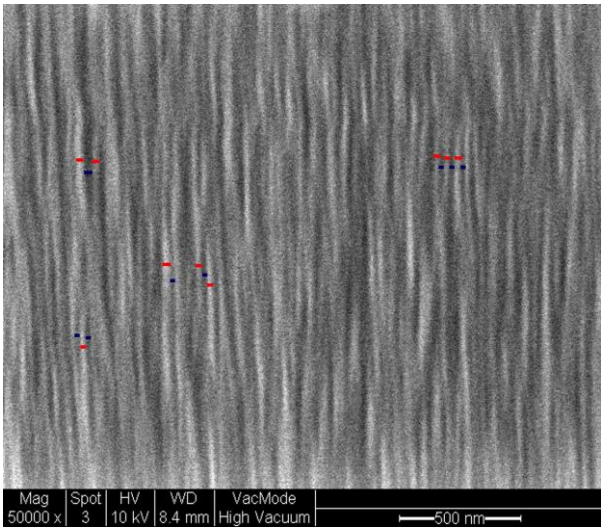

b) PWT-Por-SiC after pore wall thinning with 1 hour oxidation and 5 minute HF/ethanol dip.

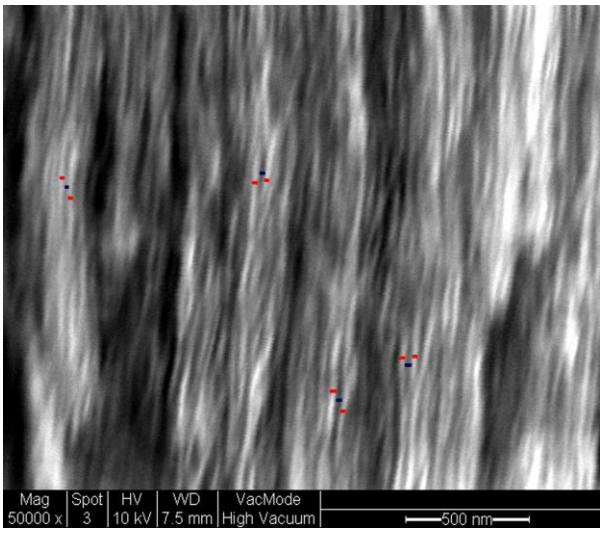

c) PWT-Por-SiC after pore wall thinning with 3 hours oxidation and 5 minute HF/ethanol dip.

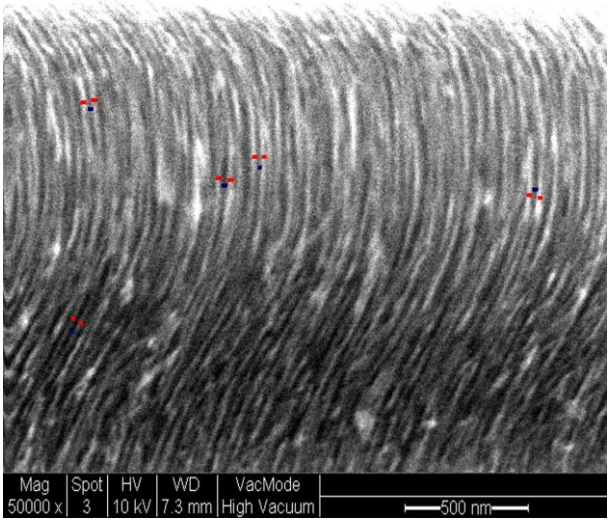

d) PWT-Por-SiC after pore wall thinning with 6 hours oxidation and 5 minute HF/ethanol dip.

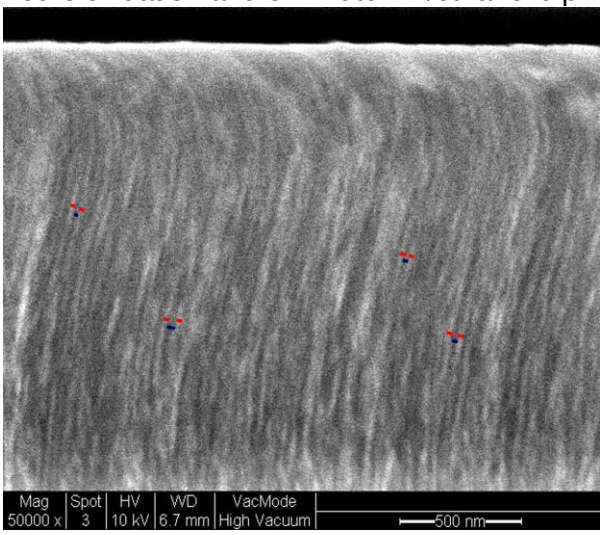

e) PWT-Por-SiC after pore wall thinning with 9 hours oxidation and 5 minute HF/ethanol dip.

Figure 2 Cross-sectional SEM images of cleaved samples showing changes in the nanocolumnar

porous morphologies over oxidation time: with indicated pore walls' thicknesses (red marks) and pore diameters (blue marks) for (a) as-etched D-Por-SiC and (b)-(e) PWT- Por-SiC with increasing oxidation times. The porous channels propagate along the [0001] direction. Scale bar: 500 nm.

A cross-sectional SEM image of a cleaved as-etched D- Por-SiC sample shows that regular vertical nanocolumnar structures were formed during the electrochemical etching (Fig. 2(a)). The self-ordered nanocolumnar structure with uniform pore wall thickness along the vertical direction of the as-etched D-Por-SiC enables a higher degree of size control in the subsequent sacrificial oxidation process. Each of the set of 20 data points of pore wall thick- nesses and pore diameters are represented by the red and blue marks on the images respectively. The average pore wall thickness of as-etched D-Por-SiC was 27.1±5.0 nm (5.0 nm being the standard deviation). The average pore diameter was 12.3±3.8 nm. After a 1 hour thermal oxidation and subsequent oxide etch in HF, the average pore wall thickness was reduced to 20.5±2.8 nm as shown in Fig. 2(b). The average pore diameter increased to 20.0±5.7 nm. High temperature oxidation at 1100°C, resulted in shape distortion along the nanocolumnar channels which caused an increase in pore diameter standard deviation.

An explanation for the observed formation of nanocolumnar SiC porous structures is that under sufficient voltage bias (20 V in this work), electrochemical etching only occurs at the pore tips (bottom of vertical channel) [9]. As etching progresses, the resistance of the cell increases from 0.5 *k*Ω to 2 *k*Ω (as measured using a Keithley 2611A source meter), highly likely due to the progress of porous layer formation. The electric field is enhanced at the pore tips during etching in comparison to the bulk of the SiC. As a result, holes are attracted to the pore tips at the SiC/electrolyte interface, away from the pore walls, resulting in vertical etching. Fast removal of the oxide by using concentrated HF ensures continuous vertical pore etching.

Fig. 2(c) shows the cross-sectional SEM image of nanocolumnar porous structure after a 3 hour oxidation treatment which resulted in further reduction of the average width to 18.2±2.9 nm. The corresponding pore diameter was 20.2±6.2 nm. Fig. 2(d) shows that a 6 hour oxidation treatment resulted in an average pore wall thickness of 17.0±1.8 nm and average pore diameter of 20.2±5.7 nm. The columnar channels shapes distorted significantly, possibly due to combined effects from high temperature treatment and subsequent handling and cleaving steps. Fig- ure 2(e) shows a cross section through a D-Por-SiC layer after 9 hours of thermal oxidation. The reduced average pore wall thickness was 15.9±1.4 nm while the average pore diameter was 20.1±5.3 nm.

Fig. 3 shows the corresponding histograms for pore wall thickness and pore diameter for as-etched D-Por-SiC and PWT-Por-SiC (after 1 hour oxidation) respectively. In comparison to the as-etched D-Por-SiC (Fig. 3(a)), the peak in the pore wall thickness distribution reduced after the 1 hour oxidation and etching (Fig. 3(c)), accompanied by a narrowing of the size distribution. It goes to show that the pore wall thickness was reduced and its uniformity improved through the sacrificial oxidation. Conversely, the pore diameter of D-Por-SiC (Fig. 3 (b)) increases after the

1 hour oxidation and etching treatment (Fig. 3 (d)) along with increase in the pore diameter distribution.

The data in Fig. 4(a) show the trends for the pore wall thickness as a function of thermal oxidation time. The rate at which the pore wall thickness reduces was highest in the first hour of oxidation (6.6 nm/hour) and decreases with longer oxidation times (1.2 nm/hour over the 9 hour duration). It was reported on oxidation of porous silicon [18, 19], that Si nanocrystallites with average diameter of 10 nm showed saturation in SiO_2 thickness at about 5 nm due to full conversion of Si into SiO_2. In this work, full conversion of SiC into SiO_2 is unlikely due to the fact that the PWT-Por-SiC were dipped in 48% HF/ethanol for 5 minutes prior to FESEM inspection, which was sufficient in removing the grown SiO_2. Sacrificial oxidation has reduced the average pore wall thickness of the as-etched D- Por-SiC by 24% after one hour of thermal oxidation and 41% after 9 hours of oxidation; achieving average pore wall thickness of 15.9 nm from the initial 27.1 nm. The oxidation rate of 6.6 nm/hour within the first hour of oxidation provides a wide process margin to control the pore wall thinning of mesoporous 4H-SiC at nanometer scale. Additionally, with increasing oxidation time the standard deviation in the pore wall thickness was reduced from 5 nm to

1.4 nm. This indicates that the sacrificial oxidation shows strong potential in narrowing down the size distribution of the pore wall. However, as shown in Fig. 4(b), the aver- age pore diameter only showed substantial increase in the first hour of oxidation time from 12.3 nm to 20.0 nm after which longer oxidation times showed relatively similar pore diameters but increased standard deviations. An in-crease in pore diameter is expected with increasing oxidation time, this trend was not observed as the pore diameters shown were affected by the shape distortion along the channels after high

temperature processing, as exhibited in the increase of the pore diameter standard deviations.

The thermal oxidation of SiC is similar to that of bulk Si, in that it occurs at the interface between the oxide film and the underlying semiconductor, where SiC is the source of Si to form SiO_2. The thermal oxidation reaction for SiC is as the following [20],

$$SiC + 1.5O_2 \rightarrow SiO_2 + CO$$

Porous materials generally exhibit a larger oxidation rate than the bulk due to larger exposed surface area [21, 22]. In bulk SiC, the crystal face plays a significant role: oxidation of the Si face has been shown to be slower than the C-face, which is ascribed to the formation of an oxy- carbide layer ($Si_4C_{4-x}O_2$) on the surface, which impede the oxidation process [23]. The exact nature of the etched D-Por-SiC surface has not yet been ascertained, however previous work indicates that the electrochemically etched SiC surface is likely to show Si depletion and be C-rich [24, 25]. Here, an amorphous layer approximately 1 nm thick- ness exists on the etched surface surrounding the pore in D-Por-SiC [16]. The chemical composition of this layer is

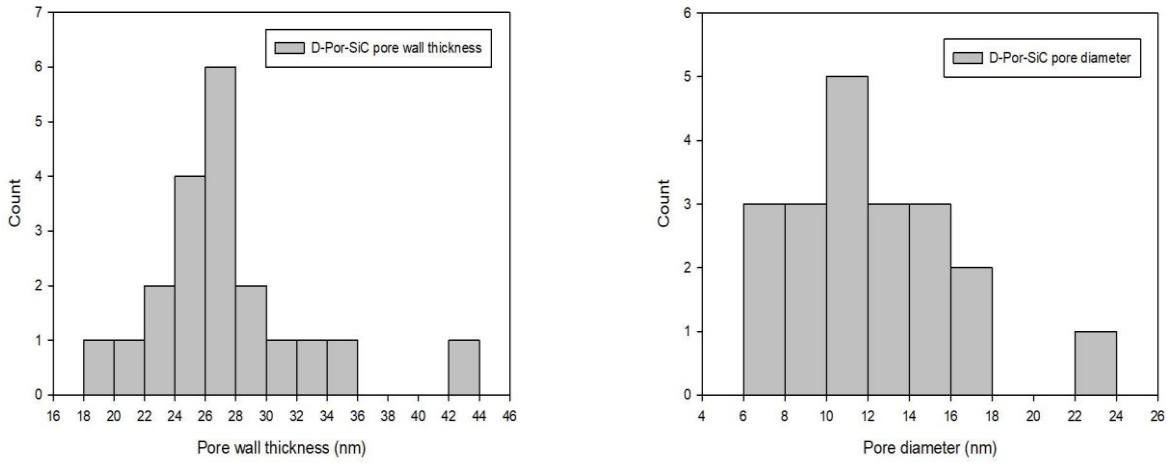

a) Histogram of pore wall thickness for D-Por-SiC. b) Histogram of pore diameter for D-Por-SiC.

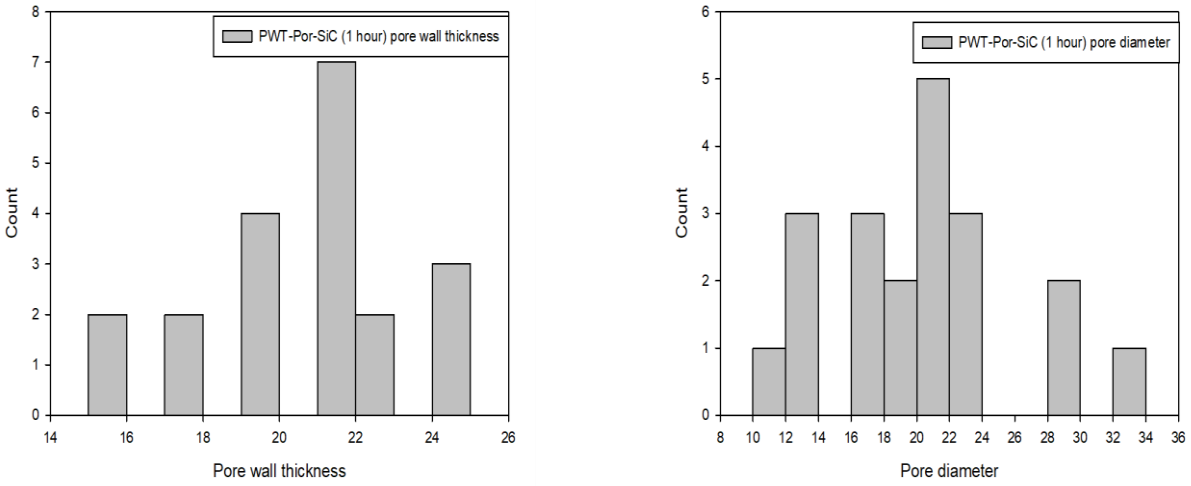

c) Histogram of pore wall thickness for PWT-Por-SiC. d) Histogram of pore diameter for PWT-Por-SiC.

Figure 3 Histogram of pore wall thickness and pore diameter for as-etched D-Por-SiC and PWT-Por-SiC (1 hour oxidation/etch).

not similar to that of the crystalline face of the bulk crystal. The formation of an amorphous layer between the crystalline SiC and pore has been reported previously [25], and the formation of which was linked to the etching conditions. Peaks related to silicon oxycarbide and SiO_2 were observed in XPS spectra [16] and these may be attributed to the existence of an amorphous layer at the surface that influence the oxidation of D-Por-SiC.

The reduced oxidation rate over time may be diffusion rate limited oxidation, influenced by the increasing distance for oxygen to diffuse through the SiO_2 and reach the SiO_2/SiC interface as oxidation progresses. Another possibility is reaction rate limited oxidation at the SiO_2/SiC interface itself. The in-diffusion of the oxidant and out- diffusion of CO through SiO_2 within the porous structure is likely the rate limiting step in this process.

In summary, within the first hour of sacrificial oxidation, pore wall thickness reduction of 24% (from 27.1 nm to 20.5 nm) and a pore wall thinning rate of 6.6 nm/hour were achieved which demonstrate a highly promising technique for controlled nanoscale size reduction in meso- porous 4H-SiC. Nanoscale size control of the pore wall would otherwise be challenging by means of electrochemical etching or ultrasonication alone imposed in part, by the wide variety of porous structures and increasing fracture energy required to break nanoscale structures. Thermal oxidation parameters that can be easily tuned with precision such as temperature and oxygen flow rate allow for process tuning and optimisation of this technique.

(a)

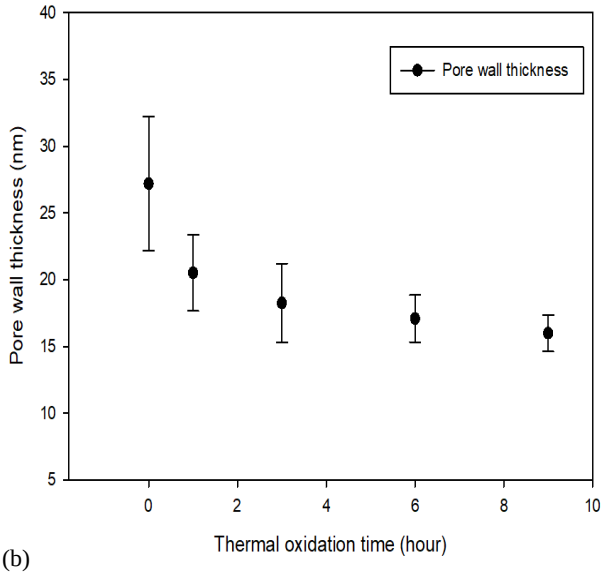

(b)

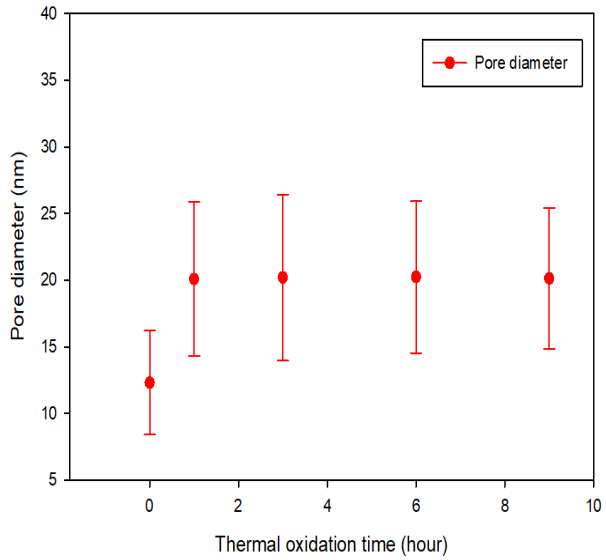

Figure 4 The mean and standard deviation of Por-SiC (a) pore wall thickness and (b) pore diameter with respect to oxidation times. The data consists of 20 data points for each oxidation time.

4 Conclusions A method of pore wall thinning of mesoporous 4H-SiC by sacrificial oxidation has been demonstrated. The nanocolumnar dimensions of electro- chemically etched mesoporous 4H-SiC are reduced during thermal oxidation in dry oxygen at 1100°C, by consuming SiC and removing the grown SiO_2 in the subsequent 48% HF/ethanol dip process. The process resulted in a reduction in the average pore wall thickness from 27 nm to approximately 16 nm within the investigated 9 hours of thermal oxidation. In addition, the size distribution improved where the pore wall thickness standard deviation reduce from ±5 nm to ±1.4 nm. The new pore wall thinning method will enable controlled nanoscale size reduction capability for mesoporous 4H-SiC derived nanostructures, that would otherwise be difficult to achieve with electrochemical etching or ultrasonication alone.

Acknowledgements We would like to thank the Ministry of Higher Education Malaysia and Universiti Sains Malaysia for the postgraduate student sponsorship.

References

[1]M. C. Roco, R. S. Williams, and P. Alivisatos, Nanotech- nology Research Directions: IWGN Workshop Report: Vi- sion for Nanotechnology in the Next Decade (Springer Sci- ence Business Media, 2000).
[2]X. Lan, S. Masala, and E. H. Sargent, Nat. Mater **13**(3), 233–240 (2014).
[3]G. Konstantatos and E. H. Sargent, Colloidal Quantum Dot Optoelectronics and Photovoltaics (Cambridge University Press, New York, 2013).
[4]X. L. Wu, J. Y. Fan, T. Qiu, X. Yang, G. G. Siu, and P. K. Chu, Physical Review Letters **94**(2), 026102 (2005).
[5]J. Fan, H. Li, J. Wang, and M. Xiao, Applied Physics Let- ters **101**(13), 131906 (2012).
[6]J. Fan and P. K. Chu, Small **6**(19), 2080–2098 (2010). [7]J. Fan, H. Li, J. Jiang, L. K. Y. So, Y. W. Lam, and P. K. Chu, Small **4**(8), 1058–1062 (2008).
[8]J. S. Shor, I. Grimberg, B. Z. Weiss, and A. D. Kurtz, Ap- plied Physics Letters **62**(22), 2836–2838 (1993).
[9]Y. Ke, R. P. Devaty, and W. J. Choyke, Physica Status So- lidi (b) **245**(7), 1396–1403 (2008).
[10]S. Askari, A. U. Haq, M. Macias-Montero, I. Levchenko, F. Yu, W. Zhou, K. K. Ostrikov, P. Maguire, V. Svrcek, and D. Mariotti, Nanoscale **8**(39), 17141–17149 (2016).
[11]E. Secret, C. Leonard, S. J. Kelly, A. Uhl, C. Cozzan, and J. S. Andrew, Langmuir **32**(4), 1166–1170 (2016).
[12]L. Zhang, V. Belova, H. Wang, W. Dong, and H. M öhwald, Chemistry of Materials **26**(7), 2244–2248 (2014).
[13]S. Gryn, T. Nychyporuk, I. Bezverkhyy, D. Korytko, V. Iablokov, V. Lysenko, and S. Alekseev, ACS Applied Nano Materials **1**(6), 2609–2620 (2018).
[14]Y. Shishkin, W. J. Choyke, and R. P. Devaty, Journal of Ap- plied Physics **96**(4), 2311–2322 (2004).
[15]Y. Ke, R. P. Devaty, and W. J. Choyke, Electrochemical and Solid-State Letters **10**(7), K24–K27 (2007).
[16]M. Rashid, B. R. Horrocks, N. Healy, J. P. Goss, and A. B. Horsfall, Journal of Applied Physics **120**(19), 194303 (2016).
[17]O. Bisi, S. Ossicini, and L. Pavesi, Surface Science Reports **38**(1-3), 1–126 (2000).
[18]G. Amato, Nanoscale Research Letters **5**(7), 1156 (2010).

[19]V. Morazzani, J. Ganem, and J. Cantin, Oxidation and nitridation of porous silicon: Comparison with compact monocrystalline silicon, (Gordon and Breach Science Publishers, 1997), pp. 481–535.

[20]Y. Song, S. Dhar, L. C. Feldman, G. Chung, and J. R. Williams, Journal of Applied Physics **95**(9), 4953–4957 (2004).

[21]T. Ito and A. Hiraki, Journal of Luminescence **57**(1), 331– 339 (1993).

[22]J. S. Shor and A. D. Kurtz, Journal of the Electrochemical Society **141**(3), 778–781 (1994).

[23]B. Hornetz, H. J. Michel, and J. Halbritter, Journal of Ma- terials Research **9**(12), 3088–3094 (1994).

[24]J. S. Shor, X. G. Zhang, and R. M. Osgood, Journal of The Electrochemical Society **139**(4), 1213–1216 (1992).

[25]S. Zangooie, P. O. A. Persson, J. N. Hilfiker, L. Hultman, and H. Arwin, Journal of Applied Physics **87**(12), 8497– 8503 (2000).